

Physical and Electrochemical Properties of Ni-P/TiN coated Ti for bipolar plates in PEMFCs

Chun Ouyang^{1,2,*}, Xinlong Zhang², Mingfang Wu¹, Damao Xun³, Pingping Gao^{4,*}

¹ School of Material Science and Engineering, Jiangsu University of Science and Technology, 212003, Jiangsu, P.R.China.

² Nantong Reshine New Materials Co., LTD. Nantong City, Jiangsu, P.R. China.

³ College of Communication and Electronics, Jiangxi Science and Technology Normal University, Nanchang, P.R.China

⁴ State Key Laboratory of Powder Metallurgy, Central South University, Changsha, 410083, P.R.China.

*E-mail: ouyc1014@163.com fengyun_gao@126.com

Received: 5 September 2019 / *Accepted:* 14 October 2019 / *Published:* 30 November 2019

Ni-P coatings including TiN nanoparticles are prepared by electroless plating on Ti plate, which is used as bipolar plates of proton exchange membrane fuel cells (PEMFCs). Scanning electronic microscope (SEM) and X-ray diffraction (XRD) are used to characterize the surface morphology and phases of the coatings, respectively. Corrosion resistance of Ni-P and Ni-P/TiN coatings are measured in the simulated solution of PEMFCs. The interfacial contact resistances (ICR) between carbon paper and bipolar plates are conducted by applied different forces. Potentiostatic polarization tests are prepared at different voltage by bubbling air and H₂ at 70 °C, respectively. It is indicated that TiN particles as a core enclosed by Ni-P are entrapped into the coating by SEM images. Comparing to Ni-P coatings, the Ni-P/TiN coating shows better behaviors of corrosion resistance and low ICR. The good corrosion resistance is attributed to the formation of coating and the compact surface morphology. Hence, Ti metal with electroless plating Ni-P/TiN coating is a potential candidate for applying in the bipolar plates of PEMFCs

Keywords: TiN nanoparticles; Electroless plating; Bipolar plates; Ni-P alloy

1. INTRODUCTION

Proton exchange membrane fuel cells (PEMFCs) are cells that use oxygen or air and hydrogen, which transform chemical energy into electrical energy [1-4]. This equipment consists of bipolar plates, electrolyte and membrane electrode assemblies[5, 6]. Among these parts, the bipolar plates play an important role in the component of PEMFCs[7]. The major barriers are the factors of cost came from the making of economic catalyst layers, solid polymer electrolyte membrane and bipolar plates. Real applied

voltage of PEMFCs is about 0.7V. The PEMFCs are always stacked in order to obtain high power. Therefore, different units of cell are connected by conductive material such as bipolar plates, which also collect current. The price of bipolar plate accounts for more than 40%-60% of total price of PEMFCs and about 80% of the total weight in fuel cell. Bipolar plates should have good corrosion resistance, good mechanical properties, high conductivity and chemical stability [8, 9].

Now the general application of material in the PEMFCs as bipolar plate is the graphite, which has high conductivity, good corrosion resistance. However it has permeability, high weight and volume [10]. Therefore, researchers around the world proposed the metal instead of graphite as the bipolar plates. The alternative metals are titanium and stainless steel [11]. The stainless steel must be covered by a highly corrosion-resistance and good conductive coating. Because the stainless steels can be released metal ion while corroded, which can poison the membrane electrode assemblies (MEA) of the electrolyte [12]. Titanium and its alloys were recognized as the most import alloy material for elsewhere application in the field of aerospace and aviation, automation and high temperature alloys [13-15]. Because the oxides were formed on the surface of Ti alloys with low electrical conductivity and poor abrasive resistance. The appropriate coating was used to improve the poor surface properties of titanium alloys. Among those morphology modification, the nickel-phosphorous coating on Ti plates had attracted more and more attention because of their better corrosion resistance, better electrical conductivity and better wear resistance [16]. Electroless plating Ni-P composite coatings incorporating TiO₂ [17], ZrO₂ [18], carbon nano-tube [19], Al₂O₃ [20], CeO₂ [21] and TiN [22-24] have been studied carefully. With addition of ceramic particles after heat treatment, the hardness and wear resistance of the coatings have been improved obviously [25]. Shibli et al. [26] concluded that the Ni-P plates with incorporation of nano-ZnO showed good corrosion resistance and improvement of metallurgical. The formation of TiN on the Ti surface were extensively studied by researchers due to their low interfacial contact resistance, good corrosion resistance and easy fabrication [27-30]. TiN-coated Ti as bipolar plates by multi-arc ion plating was investigated by Zhang et al. [31]. It was shown that the interfacial contact resistance and corrosion resistance were improved. The Ti coated TiN as bipolar plate showed good performance for single fuel cell. TiN coating on Ti by nitrogen plasma-implanted titanium was use to improved the corrosion resistance and conductivity as bipolar plates in the simulated PEMFCs enviroment [32]. Therefore, the high quality TiN film without defect was the key point for using as bipolar plates in the PEMFC fuel cells [33-36]. However, most of the former researches paid attention to the TiN coating on substrate. Few researches had ever examined the Ni-P coating on TiN nanoparticles. Therefore, the purpose of this paper is to investigate the effects of the TiN on the conductivity of Ni-P coating on Ti.

The method of electroless plating is very easy and economic to form coating on substrate in order to improve the corrosion resistance. TiN particles are good conductivity, which can enhance the conductivity after oxidation of coating in the acid environment of PEMFCs. The wear resistance of coating can be improved by the adding of TiN nano-particles in the electroless plating of Ni-P. Therefore, nano-composite coating on Ti are prepared in our work. Based on the electroless plating model and theories of crystal growth, the effects of the TiN nanoparticles on coating were explored too. The substrate with coating will be candidate for bipolar plates in the environment of PEMFCs.

2. EXPERIMENTAL

The commercial pure titanium was used as the matrix metal in our research. Its composition (wt.%) was 0.3 Fe, 0.15 Si, <0.1 C, <0.05 N, <0.015 H, <0.2 O, Ti balance. The TiN were purchased from Aladdin Corporation with a size of 50 nm in diameter in Shanghai city. The Ti plate were cut into a square (20 mm×20 mm×2mm). The treated Ti was ultrasonicated for more than 10 min and was cleaned in distill water. Before electroless plate, the oxide layer of TiO₂ must be removed chemically for 5 min.

The bath solution of Ni-P electroless plating was prepared, which contained 35 g/L Ni₂SO₄·6H₂O, 20 g/L NaH₂PO₄·H₂O, 30 g/L C₆H₅O₇Na₃·2H₂O, 40 g/L NH₄Cl. The pH of solution keep 8 adjusted by NH₃·H₂O. The temperature of bath was kept at 85 °C in the process of electroless plating. The TiN nanoparticles (1.0 g/L) were added into the solution by ultrasonification and magnetic stirring in order to obtain the uniform suspension. Then, the Ti sheets were placed in the mix solution of eletroless plating with and without addition of TiN nanoparticles. After electroless plating, the prepared coatings were washed by distill water and dried by air. Then the coatings were heat treated for 2 h (at the temperature of 400 °C).

Polarization measurements were carried out in a simulated solution (0.5 M H₂SO₄+ 2 ppm NaF) at working temperature (=70 °C). The Ti sheets with coatings were as working electrode with a sweep rate of 1 mV/s and volt range from -0.8 V to 0.8 V. A saturated calomel electrode (SCE) was used as a reference electrode. Pt sheet with surface area of 1 cm² was used as a counter electrode. Potentiostatic polarization was carried out in the simulated environment of PEMFCs for 5 h at 70 °C, while bubbling air at the potential of 0.6 V(vs. SCE) and bubbling H₂ at the potential of -0.1 V(vs. SCE), respectively.

Two pieces of carbon paper were sandwiched between the specimen and two copper plates. The ICR values were obtained by applying different compaction forces. The coating was washed with acetone and distill water for several times. Scanning electron microscope (SEM) was used to characterize the surface morphology. Energy dispersive spectroscopy (EDS) was used to anylyze the element from spots or area of sample. The phase of coating on Ti is charactized by the X-ray diffraction (XRD) with Cu K α radiation. A step of 0.02° was used to scan from 10° to 95° with a step time of 1 s.

3. RESULTS AND DISCUSSION

3.1 The effect of TiN on the coating

Fig. 1 shows the XRD patterns of the four coatings before and after heat treatment at different temperature. Fig. 1a shows the XRD patterns of specimens and Ni-P coatings without and with TiN particles deposited for 2.5 h. There is a broad peak at 45° in the coating of Ni-P which is related to the amorphous crystal of Ni-P coating. Fig. 1b shows the XRD patterns of as-deposited coatings with Ni-P/TiN and the specimens are heat treated at 200 °C and 400 °C, respectively. The Ni, Ni₃P and NiP phases are formed from the amorphous Ni-P coating after heat treatment at 400 °C. Simultaneously, the surface morphology is influenced by the content of TiN nanoparticles[37].

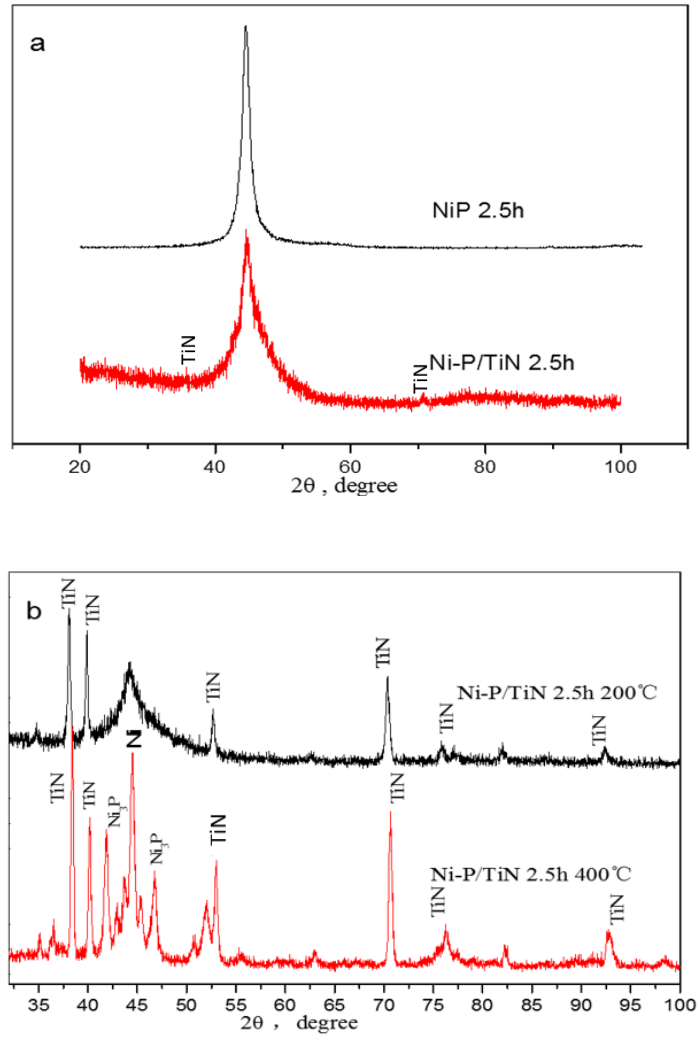
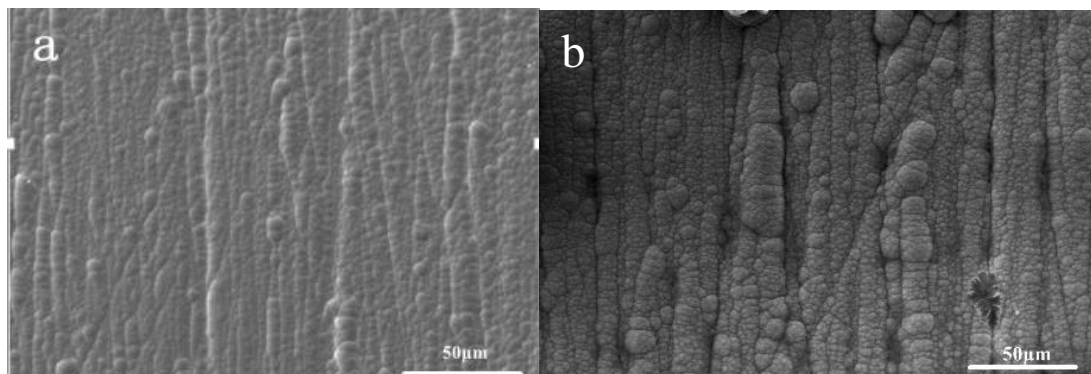


Figure1. XRD pattern of Ni-P and Ni-P/TiN coating deposited for 2.5 h before and after heat treatment (a) Ni-P, Ni-P/TiN coating before heat treatment (b) heat treatment at 200°C, 400°C, respectively on Ni-P/TiN coating.



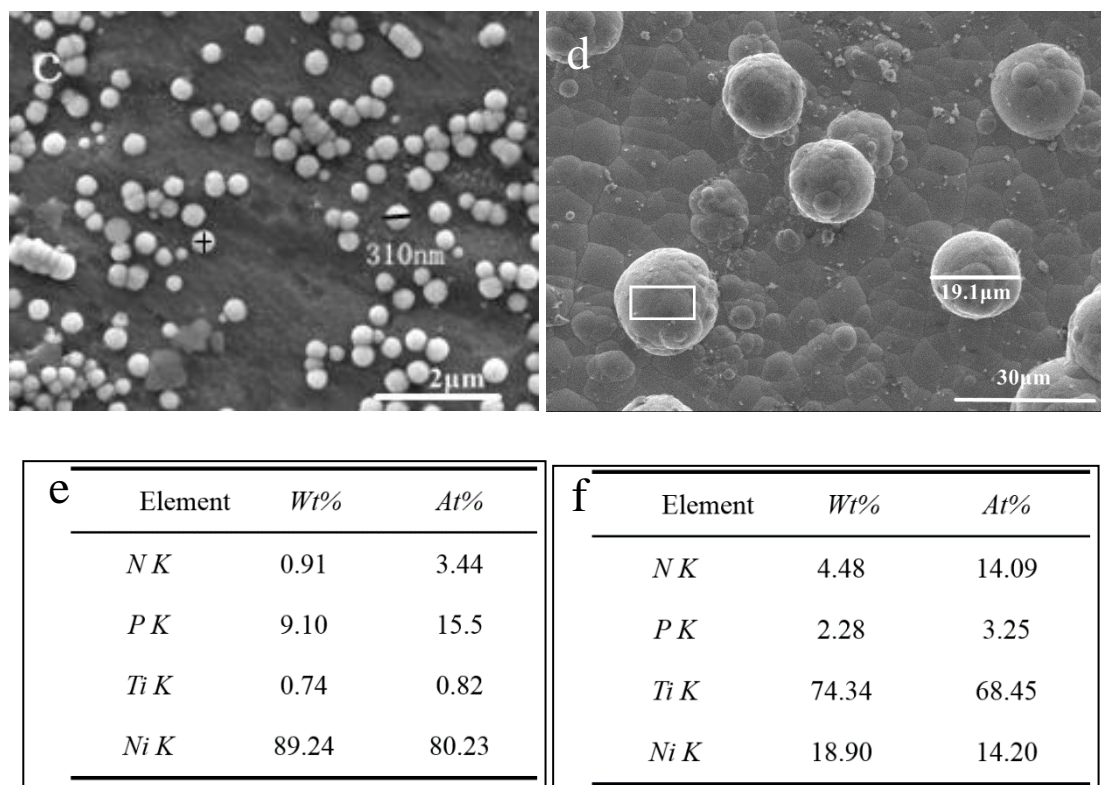


Figure 2. SEM images and EDS analysis of coating after heat treatment at 400 °C within 2h for different deposition times (a) 0.5 h without TiN (b) 2.5 h without TiN (c) 0.5 h with TiN (d) 2.5 h with TiN (e) EDS analysis from the cross in Fig. 2c (f) EDS analysis from the rectangular region in Fig. 2d

Fig. 2a and 2b show the surface morphology of Ni-P coating without TiN nanoparticles for deposition at 0.5 h and 2.5 h respectively. From Fig. 2a and 2b, it can be seen that the grains of Ni-P are deposited uniformly and homogeneously with a size of 1~4 μm. The Ni-P coatings show a refined nodular structure. Fig. 2b shows less compact nodule-like structure with larger time of deposition comparing to Fig. 2a. The grain size is bigger with large time of deposition in Fig. 2b comparing to the size in Fig. 2a. The P element is one of the good effect of reducing the cracking while electroless plating. After 2.5 h deposition, the region between nodular-like crystalline exhibits crack because of compressive stress base on the surface stress model [38-40]. The surface of Ti substrate is covered by flat surface compact structure after electroless plating. Fig. 2c and 2d show the SEM images of Ni-P coatings with TiN nanoparticles deposited for 0.5h and 2.5h, respectively. After deposition for 0.5 h, parts of TiN particles are enclosed by Ni-P electroless plating. The enclosed TiN are entrapped into the Ni-P coating. The average diameter of the enclosed particles are up to 310 nm shown in Fig. 2c, which is 6 times than the original size. After deposition for 2.5 h, the average diameter of the enclosed particles are up to 19.1 μm shown in Fig. 2d, which is 400 times comparing with the original size. The crystallite sizes are influenced by the site of nucleation [21, 38, 39]. It can be concluded that the nanoparticles are adsorbed on the surface of Ti sheet as the nucleation center, which accelerates the Ni-P deposition comparing with the size of ball in Fig. 2c and 2d, respectively. The main elements are Ni and P, which are determined by the Ni-P electroless plating.

The elements N and Ti come from the core of TiN nanoparticles. The normal diameter of the commercial TiN nanoparticles is roughly 50 nm. There is not a long nodules-like structure in Fig. 2c and 2d comparing to that of the only Ni-P coatings on the surface of substrate in Fig. 2a and 2b. From the EDS analysis of the black cross in Fig. 2c and the rectangular region in Fig. 2f, the content of Ni-P increases greatly, which means that the shell structure is consist of Ni-P coating. The results are coincide to the change of diameter of ball on the surface substrate. The more sites of nucleation are formed on the surface of substrate. The grains are formed while the grain growth is restrained. Then grains are finer than that of Ni-P coating[40]. In order to research the interface content of TiN nanoparticle, the TiN particles enclosed by Ni-P plating are incorporated into the coatings from the results of EDS analysis in the rectangular region of Fig. 3a. The close combination of coating and substrate will provide good corrosion resistance and TiN nanoparticles will be benefit for the conductivity of coating as the bipolar plates of PEMFCs [41]. The thickness of coating is 31.2 μm roughly shown in Fig. 3a. The coating is consist of Ni-P coating with TiN particles from the elements distribution of N, P, Ti and Ni in Fig. 3b.

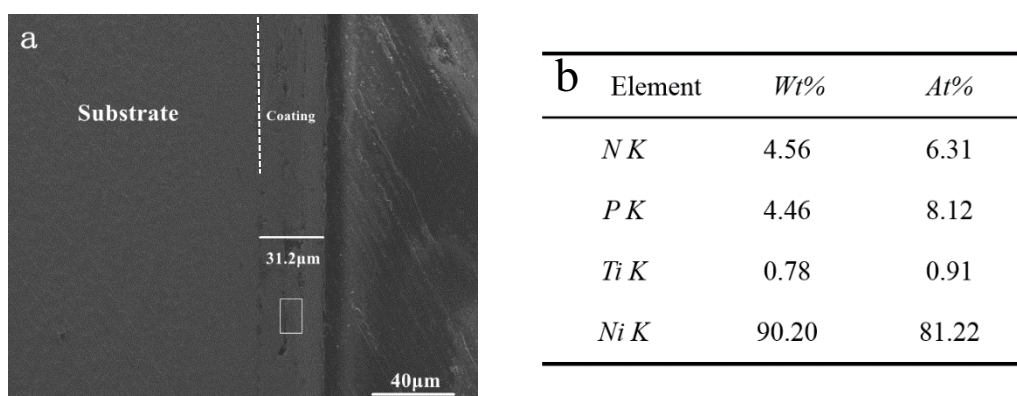


Figure 3. SEM images and EDS analysis of coating for 2.5 h deposition

3.2 The effect of TiN on corrosion resistance of coating

From the above analysis, the surface morphology is influenced by the TiN nano-particles. Furthermore, the corrosion resistance of the coating is influenced by the surface morphology. The method of potentiodynamic polarization is used to test the corrosion resistance of coating. Fig. 4 shows the potentiodynamic polarization curves of bare Ti and coatings after heat-treatment. The values of corrosion current density and corrosion potential are calculated from the polarization curve by using the Tafel extrapolation method, as shown in Table 1. The corrosion current density of bare Ti and Ni-P coating is $20.1 \mu\text{A}\cdot\text{cm}^{-2}$ and $13.8 \mu\text{A}\cdot\text{cm}^{-2}$, respectively. With the addition of TiN particles, the value of corrosion current decrease obviously. In the case of Ni-P/TiN coating deposited for 0.5 h, the value of current density is $1.12 \mu\text{A}\cdot\text{cm}^{-2}$. In the case of Ni-P/TiN coating deposited for 1.5 h, the current density is $1.01 \mu\text{A}\cdot\text{cm}^{-2}$, similar to Ni-P/TiN coating deposited for 0.5 h. These results indicate that the addition of TiN nanoparticles improve the corrosion resistance of coating in the simulated environment of PEMFCs. It is well known that P plays a key role on the film of surface passivation. The coating including adsorbed hypophosphite anions will hinder the further hydration of nickel[40]. The TiN

particles will be helpful for accelerating deposition of Ni-P[42]. After deposition for 2.5 h, the value of current density decreases to $0.206 \mu\text{A}\cdot\text{cm}^{-2}$. The corrosion resistance meets the Department of Energy's (DOE) 2020 technological target in USA (current density $<1 \mu\text{A}\cdot\text{cm}^{-2}$). This result shows that the TiN nanoparticles are in favor of forming compact coating to improve the corrosion resistance.

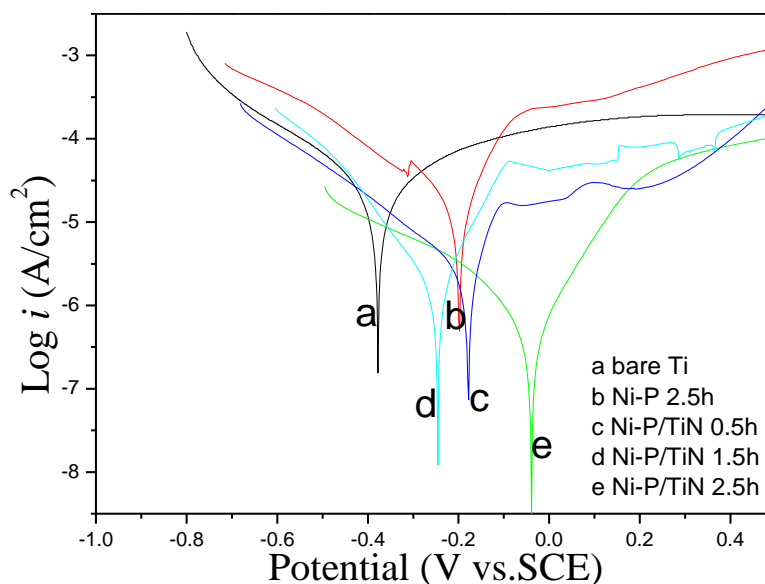


Figure 4. Potentiodynamic polarization curves of the coatings and bare Ti after heat-treatment in 0.5 M H_2SO_4 and 2 ppm NaF solution at 70°C with bubbling air.

Table 1. Calculation values of corrosion current density and corrosion potential measurement from Fig. 4 after heat treatment at 400°C .

Coating	$E_{corr.}$ (V vs.SCE)	$i_{corr.}$ ($\mu\text{A cm}^{-2}$)
bare Ti	-0.354	20.1
Ni-P 2.5h	-0.196	13.8
Ni-P/TiN (0.5h)	-0.174	1.12
Ni-P/TiN (1.5h)	-0.243	1.01
Ni-P/TiN (2.5h)	-0.042	0.206

In order to investigate the stability of the coating, EIS measurements are conducted by Nyquist plots shown in Fig. 5. Table 2 shows the electrochemical parameters obtained from simulated equivalent circuits from Fig. 5. There is one time constant for all specimens because all plots are simple semi-circle[43]. The impedance spectra was fitted by the equivalent electrical circuit as shown in Fig.5. Electrochemical parameters are obtained from Nyquist plots fitted by equivalent electrical circuit. In the table 2, n is an adjustable parameter as a CPE power between 0.5 and 1. When $n=1$, the CPE is defined an ideal capacitor. When $n=0.5$, the CPE represents a Warburg impedance. For $0.5 < n < 1$, the CPE represents a distribution of dielectric relaxation times in frequency space. R_s represent the electrolyte resistance. Q is the pseudocapacitance of the film. R_f represents the resistance of film. The film resistance

of Ni-P/TiN is larger than that of Ni-P coating for 0.5 h deposition time. The film resistance (R_f) of Ni-P/TiN after heat treatment increases as the increase of deposited time. The value of film resistance increase from about $1520 \Omega \cdot \text{cm}^{-2}$ to $3760 \Omega \cdot \text{cm}^{-2}$ after the addition of TiN nanoparticles deposition for 2.5 h after heat treatment at 400°C . The effect of TiN on Ni-P coating is to accelerate the deposition of Ni-P, indicating that the Ni-P/TiN shows the best performance of anti-corrosion with 2.5h deposition after heattreatment.

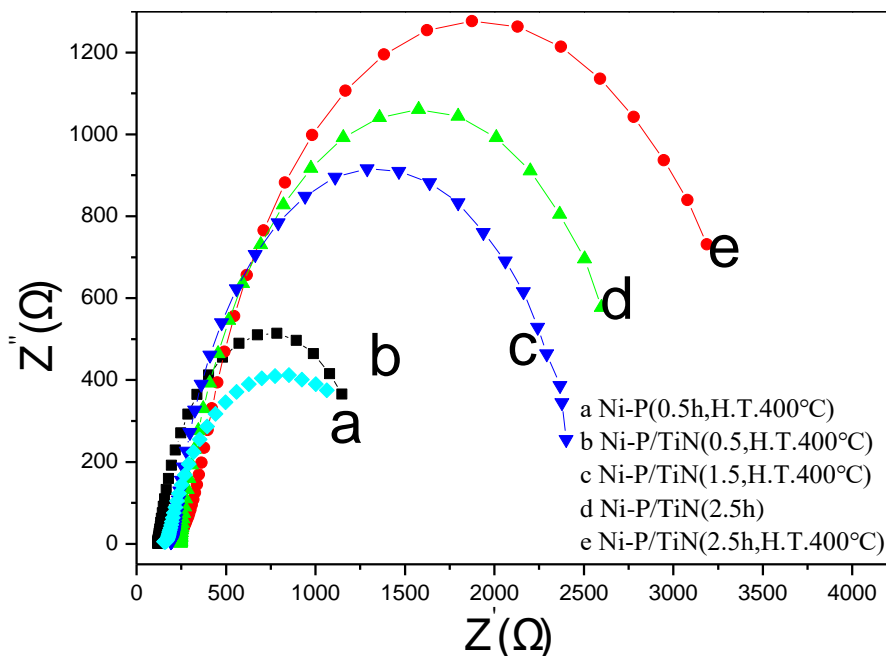


Figure 5. Nyquist plots and equivalent circuits of the corrosion condition for Ni-P and Ni-P/TiN coating in 0.5 M H_2SO_4 and 2 ppm NaF solution

Table 2. Electrochemical parameters obtained from simulated equivalent circuits in Figure5

Coating	n	$R_{sol}/\Omega \text{ cm}^{-2}$	$Q/\Omega^{-1} \text{ s}^n \text{ cm}^{-2}$	$R_f/\Omega \text{ cm}^{-2}$
a	0.8	120.0	6.17×10^{-4}	1.28×10^3
b	0.8	162.8	5.15×10^{-4}	1.52×10^3
c	0.82	197.6	4.24×10^{-4}	2.35×10^3
d	0.82	245.8	1.72×10^{-4}	2.67×10^3
e	0.76	247.8	7.52×10^{-5}	3.76×10^3

In order to investigate the stability of Ni-P/TiN coating on Ti as bipolar plates, potentiostatic polarization is conducted for 5 h in 0.5 M $\text{H}_2\text{SO}_4 + 2$ ppm NaF solution at 70°C as shown in Fig. 6. The results of measurement for coating in bubbling air and H_2 as working electrode in the environments of PEMFCs are shown in Fig. 6a and 6b, respectively. In such simulated anode environment of PEMFCs, Ni-P/TiN coating shows the lowest corrosion current density comparing to that of bare Ti and Ni-P coating in Fig. 6a. In such simulated cathode environment of PEMFCs, Ni-P/TiN coating also shows the lowest corrosion current density comparing to that of bare Ti and Ni-P coating in Fig. 6b. The transient

current density decays quite fast in the very early stage while bubbling air. Then the current density of Ni-P/TiN is 2.1×10^{-7} A/cm², which keeps stable last for a long time. This implies that the surface is covered by passive film at the beginning time. The current density of Ni-P/TiN coating is roughly -1.52×10^{-6} A/cm² in the last stage in Fig. 6b while bubbling H₂, which was due to the H⁺ reduction to H₂. The coating is under the protection of cathode [44]. It is also found that Ti bipolar plates with coating are effectively protected by coating without severe corrosion.

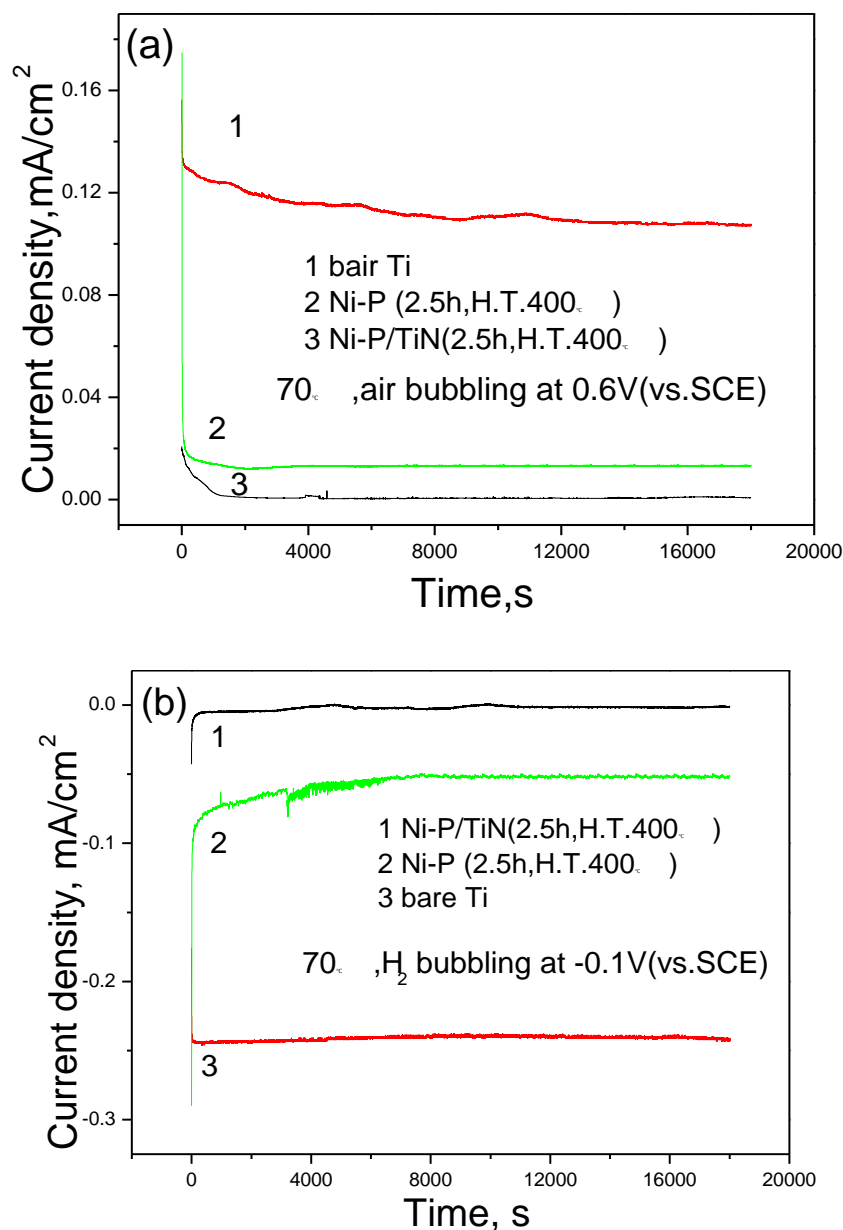


Figure 6. Potentiostatic polarization patterns of bare Ti and the coatings after heat-treatment at 400 °C (a)Ti, Ni-P and Ni-P/TiN with bubbling air for 5h (b) Ti, Ni-P and Ni-P/TiN with bubbling H₂ for 5 h.

3.3 The effect of TiN on the conductivity

All ICR measurements are conducted after the potentiostatic polarization for 5 h at 0.6 V. The Interfacial contacting resistance between the coating and the carbon paper is shown in Fig. 7. The applied forces are from 60 to 220 N/cm². It is clearly indicated that the resistance decrease with the increase of applied force in four specimens, which cause by the increase of contacting area. The ICR values for Ni-P coating on the Ti are larger than the Ti with Ni-P/TiN coatings. At the force of 60 N/cm², the values of ICR drop from 82.5 mΩ·cm² to 30.3 mΩ·cm², implying that the conductivity of the coating has improved obviously by addition of TiN nanoparticles. The ICR decrease with increase of time of deposition. Under the applied force of 140 N/cm², the ICR values of Ni-P/TiN coating for 0.5h, 1.5h and 2.5h are 8.7, 6.2 and 3.5 mΩ·cm², respectively which meet the require of DOE's 2020 targets (ICR <10 mΩ·cm²). After further increase of applied force, the ICR values of these three coatings are almost stable under 10 mΩ·cm²). The Ni-P coating on Ti is favor of preventing from the formation of TiO₂, which is insulator. At the same time, the lower charge transfer resistance in Table. 2 provides the better charge transfer kinetics. Therefore, the TiN nano-particles in coating give rise to the electronic conductivity and charge transfer kinetics together. According to the results of ICR, it can be concluded that the conductivity of Ti plates with coating is greatly improved by addition TiN nano-particles into Ni-P electroless plating after polarization process.

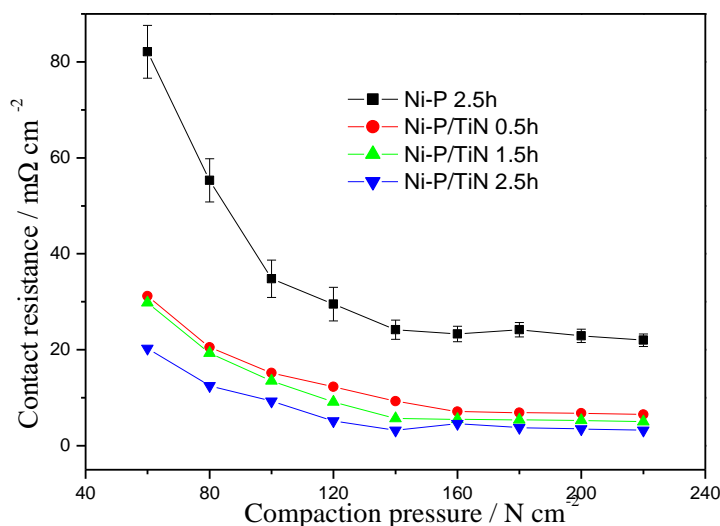


Figure 7. Interfacial contact resistance between the specimens and carbon paper under different compaction press after polarization tests in air for 5 h.

Fig. 8a shows the schematic diagram of the current path between bare Ti and the carbon paper. Fig. 8b and 8c show the schematic diagram of the current path between the coating and the carbon paper. Fig. 8d shows the method of measurement of interfacial contact resistance. With the increase of pressing force, the contact area will increase obviously. In this stage, the contact area is the key factor for the decrease of contact resistance. The discrepancy of surface morphology can be neglected by using carbon paper as conductor. Fig. 8a shows the current paths on Ti metal with TiO₂ thin layer. The Ni-P coating

on Ti will generate more paths comparing with the conductivity of Ni element, which reduce the interfacial contact resistance. Because of the better conductivity of TiN than Ni-P coating, the current flow of coating with the addition of TiN is easier than that of the only Ni-P coating. The electrical conductivity of Ni-P/TiN is improved by the addition of TiN.

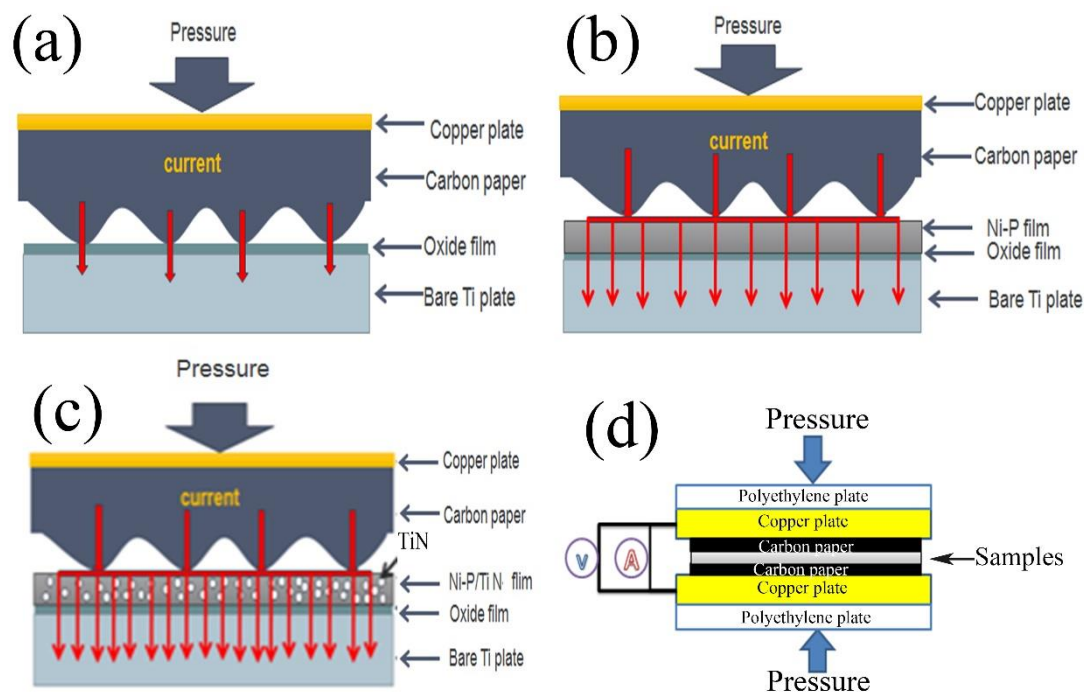


Figure 8. Schematic diagram of current path between coating and carbon (a) bare Ti (b) Ni-P coating on Ti (c) Ni-P/TiN coating on Ti (d) ICR test model.

3.4 The effect of TiN on surface morphology after potentiostatic polarization

Fig.9 shows the surface morphology after potentiostatic polarization of coatings in the simulated solution at 70°C while bubbling air and H₂. Fig. 9a and 9b show morphology of Ni-P coatings after polarization for 5 h with bubbling H₂ at -0.1V (vs.SCE) and with bubbling air at 0.6 V (vs. SCE), respectively. Fig. 9c and 9d show morphology of Ni-P/TiN coatings after polarization for 5 h with bubbling H₂ at -0.1V (vs. SCE) and with bubbling air at 0.6V (vs. SCE) respectively. Comparing with the Ni-P coating in Fig. 9b, the grain of Ni-P/TiN is bigger in Fig. 9d. In the case of polarization potential at 0.6 V, the grain boundary of coatings is corroded. The pinholes are generated around the grain boundary in Fig. 9b and 9d. In the case of the Ni-P coating including TiN particles, the surface morphology is more dense and intact after polarization at -0.1V in Fig. 9c comparing to the Ni-P coating in Fig. 9a. The TiN nanoparticles affect the growth of grain of Ni-P as acting a nucleating site in the process of electroless plating. The TiN nanoparticles are distributed evenly in the coating and inhibit the diffusion of Ni²⁺ ions[45]. However, the surface morphology is litter corroded after polarization at 0.6 V in Fig. 9d. It implies that extent of corrosion in the simulated air-bubbling environment is severer

than that in H₂-bubbling environment. The honeycomb-like morphology is formed by the dropped ball, which don't destroy the integrity of coating. The honeycomb-like surface increases the contacting area with carbon paper, which decrease interfacial contacting resistance. Without obviously crack or debris, the Ni-P coatings with TiN particles can prevent from penetration of electrolyte into inner parts of coating or substrate.

To summarize, the Ni-P/TiN coatings shows better anti-corrosion and better stability in simulated solution of PEMFCS than that Ni-P coating on Ti.

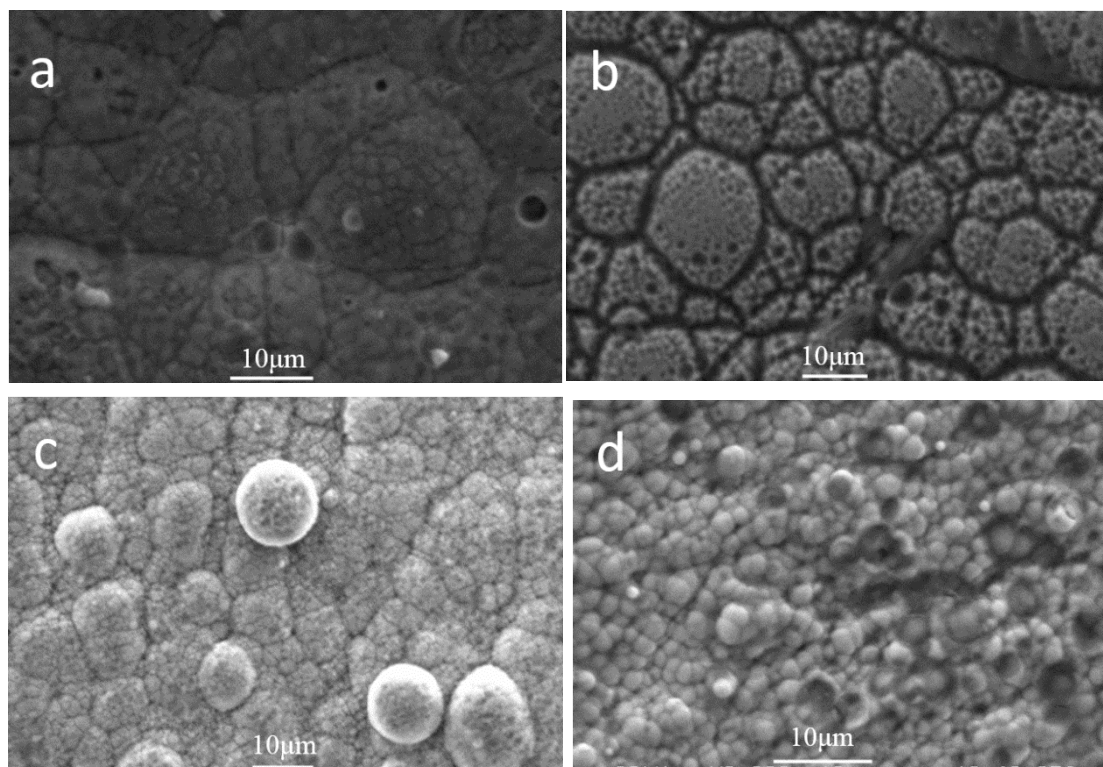


Figure 9. Surface morphology of coatings after potentiostatic polarization test in simulated solution at 70°C for 5 h (a) Ni-P coating while bubbling H₂ at -0.1 V (b) Ni-P coating while bubbling air at 0.6 V (c) Ni-P/TiN coating while bubbling H₂ at -0.1 V (d) Ni-P/TiN coating while bubbling air at 0.6 V.

4. CONCLUSIONS

The Ni-P/TiN coatings are prepared in this paper to improve the conductivity and corrosion resistance of Ti metal bipolar plates used in PEMFCs. Both of the films including Ni-P and Ni-P/TiN show smooth morphology. The TiN nanoparticles are distributed evenly. TiN particles as nucleus are enclosed and entrapped by Ni-P electroless plating. The Ni-P/TiN coatings on Ti shows better anti-corrosion and conductivity comparing with Ni-P coating. The better corrosion resistance is attributed to the intact film with few of cracks. That is because of TiN as nucleus to accelerate the formation of Ni-P

coating on Ti. The better conductivity of the coating comes from the addition of TiN particles, which has good conductivity and reduce the interfacial conductivity at high applied potential after potentiostatic polarization tests for 5 h. Ti bipolar plates with Ni-P/TiN coating will be a promising candidate for bipolar plates of PEMFCs.

ACKNOWLEDGEMENTS

This research was funded by [Jiangsu Province Post Doctoral Fund, 2018.9], [Natural Science Foundation of Jiangsu Province, BK20190973] and [the Fund for Distinguished Young Scholars of Jiangxi Science and Technology Normal University, 2016QNBjrc0006], The authors gratefully acknowledge my supervisor Prof. Ting Lei for data discussiong.

References

1. R. Anderson, L. Zhang, Y. Ding, M. Blanco, X. Bi, D.P. Wilkinson, *Journal of Power Sources*, 195 (2010) 4531.
2. J.F. Lin, V. Kamavaram, A.M. Kannan, *Journal of Power Sources*, 195 (2010) 466.
3. Y. Li, J. Yang, J. Song, *Renewable and Sustainable Energy Reviews*, 67 (2017) 160.
4. D. Chen, Q. Zeng, S. Su, W. Bi, Z. Ren, *Applied Energy*, 112 (2013) 1100.
5. S.J. Peighamardoust, S. Rowshanzamir, M. Amjadi, *International Journal of Hydrogen Energy*, 35 (2010) 9349.
6. Y. Yu, H. Li, H. Wang, X.Z. Yuan, G. Wang, M. Pan, *Journal of Power Sources*, 205 (2012) 10.
7. S.P. Jung, C.I. Lee, C.C. Chen, W.S. Chang, C.C. Yang, *Journal of Power Sources*, 283 (2015) 429.
8. H. Luo, H. Su, C. Dong, K. Xiao, X. Li, *Journal of Alloys & Compounds*, 686 (2016) 216.
9. S.P. Mani, A. Srinivasan, N. Rajendran, *International Journal of Hydrogen Energy*, 40 (2015) 3359.
10. C. Du, P. Ming, M. Hou, J. Fu, Y. Fu, X. Luo, Q. Shen, Z. Shao, B. Yi, *Journal of Power Sources*, 195 (2010) 5312.
11. S.-P. Jung, C.-I. Lee, C.-C. Chen, W.-S. Chang, C.-C. Yang, *Journal of Power Sources*, 283 (2015) 429.
12. M. Kumagai, S.T. Myung, R. Asaishi, Y.K. Sun, H. Yashiro, *Electrochimica Acta*, 54 (2008) 574.
13. J. Luo, M. Li, X. Li, Y. Shi, *Mechanics of Materials*, 42 (2010) 157.
14. Y.S. Tian, C.Z. Chen, S.T. Li, Q.H. Huo, *Applied Surface Science*, 242 (2005) 177.
15. Y. Qiao, X. Cai, J. Cui, H. Li, *Advances in Materials Science and Engineering*, 2016 (2016).
16. C. Gao, L. Dai, W. Meng, Z. He, L. Wang, *Applied Surface Science*, 392 (2017) 912.
17. V. Uttam, R.K. Duchaniya, Potentiodynamic studies of Ni-P-TiO₂ nano-composited coating on the mild steel deposited by electroless plating method, 2016, pp. 219.
18. Y. Yang, W. Chen, C. Zhou, H. Xu, W. Gao, *Applied Nanoscience*, 1 (2011) 19.
19. F.Z. Kong, X.B. Zhang, W.Q. Xiong, F. Liu, W.Z. Huang, Y.L. Sun, J.P. Tu, X.W. Chen, *Surface & Coatings Technology*, 155 (2002) 33.
20. S.H. Jiang, J.Y. Zhang, J.H. Liu, *Heat Treatment of Metals*, 11 (2002).
21. X. Zhou, C. Ouyang, *Surface and Coatings Technology*, 315 (2017) 67.
22. H.M. Zhou, Y. Jia, J. Li, X.Y. Hu, 36 (2015) 192.
23. X. Shi, L. Xu, T.B. Le, G. Zhou, C. Zheng, K. Tsuru, K. Ishikawa, *Materials Science and Engineering: C*, 59 (2016) 542.
24. X. Shi, L. Xu, M.L. Munar, K. Ishikawa, *Materials Science and Engineering: C*, 49 (2015) 1.
25. X. Wang, R. Wu, X. Ren, J. Feng, W. Pan, *Rare Metal Materials & Engineering*, 40 (2011) 478.
26. S.M.A. Shibli, B. Jabeera, R.I. Anupama, *Applied Surface Science*, 253 (2006) 1644.
27. C.K. Jin, M.G. Jeong, C.G. Kang, *International Journal of Hydrogen Energy*, 39 (2014) 21480.

28. M. Omrani, M. Habibi, M.S. Moti Birjandi, *International Journal of Hydrogen Energy*, 41 (2016) 5028.
29. S. Wang, M. Hou, Q. Zhao, Y. Jiang, Z. Wang, H. Li, Y. Fu, Z. Shao, *Journal of Energy Chemistry*, 26 (2016).
30. M. Kumagai, S.-T. Myung, R. Asaishi, Y.-K. Sun, H. Yashiro, *Electrochimica Acta*, 54 (2008) 574.
31. D. Zhang, L. Duan, L. Guo, Z. Wang, J. Zhao, W.H. Tuan, K. Niihara, *International Journal of Hydrogen Energy*, 36 (2011) 9155.
32. K. Feng, D.T.K. Kwok, D. Liu, Z. Li, X. Cai, P.K. Chu, *Journal of Power Sources*, 195 (2010) 6798.
33. R. Tian, J. Sun, *International Journal of Hydrogen Energy*, 36 (2011) 6788.
34. M. Omrani, M. Habibi, R. Amrollahi, A. Khosravi, *International Journal of Hydrogen Energy*, 37 (2012) 14676.
35. L.T. Duan, D.M. Zhang, L. Guo, Z.Y. Wang, *Chinese Journal of Nonferrous Metals*, 21 (2011) 159.
36. K. Feng, Z. Li, *Thin Solid Films*, 544 (2013) 224.
37. P. Gao, Z. Xie, C. Ouyang, T. Tao, X. Wu, Q. Huang, *Journal of Solid State Electrochemistry*, (2018) 1.
38. M.E. Hyde, R.G. Compton, *Journal of Electroanalytical Chemistry*, 581 (2005) 224.
39. X. Zhou, C. Ouyang, *Applied Surface Science*, 405 (2017) 476.
40. J. Hu, L. Fang, P.-W. Zhong, *Materials and Manufacturing Processes*, 28 (2013) 1294.
41. H. Kim, M.K. Cho, J.A. Kwon, Y.H. Jeong, K.J. Lee, N.Y. Kim, M.J. Kim, S.J. Yoo, J.H. Jang, H.J. Kim, *Nanoscale*, 7 (2015) 18429.
42. P. Gao, C. Ouyang, Z. Xie, T. Tao, *Surface Review & Letters*, 25 (2017).
43. S. Ranganatha, T.V. Venkatesha, K. Vathsala, *Applied Surface Science*, 256 (2010) 7377.
44. L. Wang, J. Sun, J. Sun, Y. Lv, S. Li, S. Ji, Z. Wen, *Journal of Power Sources*, 199 (2012) 195.
45. I.R. Mafi, C. Dehghanian, *Applied Surface Science*, 258 (2011) 1876.